Electronic Supplementary Material (ESI) for Journal of Materials Chemistry A.

Supporting Information

Vampire bat's tongue-inspired superhydrophilic flexible origami channel for directional and spontaneous liquid manipulation

Zhihang Ye[a]ł, Jingyi Zhao[a]ł, Qianrui Tong[a], Xinsheng Wang[a], He Sun[a],Haoyu Bai[b], Kesong Liu[d], Moyuan Cao[ac*]*

a. School of materials science and engineering, Smart sensing interdisciplinary science centre, Nankai university, Tianjin 300350, P.R. China. Email: mycao@nankai.edu.cn

b. School of chemical engineering and technology, Tianjin university, Tianjin, 300072, P. R. China.

c. Tianjin key laboratory of metal and molecule-based material chemistry, Tianjin 300192, P. R. China.

d. School of chemistry, Beihang university, Beijing 100083, P.R. China.

ł Equal contributions footnote.

Supplementary Text:

The modeling of the apex angle changes during the topological folding process

As illustrated in Fig. S11, we postulate that three conditions remain constant during the folding process: the position of the origami's midline is invariant, the length of the origami's midline is unaltered, and the thickness of the origami does not vary throughout the folding process. Consequently, although the angle of the origami structure changes, the adjusted angle after folding can still be calculated. Firstly, as the arc length does not change after folding, the thickness of the initial origami and average radius of the origami after folding can be described as Equation 1 and 2.

$$b = a\cos\left(\frac{\alpha}{2}\right) \quad (1)$$

$$R = n\cdot\frac{a\sin(\frac{\alpha}{2})}{\pi} \quad (2)$$

where a is the length of the single channel's side, α and b represent the apex angle and the thickness of initial origami, respectively. R is the average radius of the origami after folding process, and n is the number of the channels. Therefore, after folding process, the radius of the inner circle and the outer circle can be expressed as R_1 and R_2, respectively. Further, according to the law of cosine, the folded apex angle can be further described as Equation 3-5.

$$R_1 = R + \frac{b}{2} \quad (3)$$

$$R_2 = R - \frac{b}{2} \quad (4)$$

$$\cos\left(\frac{\beta}{2}\right)=\frac{a^2+R_1^2-R_2^2}{2aR_1} \quad (5)$$

In addition, to explore the relationship between the apex angle of the SFOC surface and the folding angle, we consider scenarios where the folding angle is less than 360 degrees. Assuming the folding angle is denoted by ϑ, the average radius can be described as Equation 6.

$$R=n\cdot\frac{a\sin(\frac{\alpha}{2})}{\pi}\cdot\frac{360}{\theta} \quad (6)$$

Based on this equation, assuming a fixed apex angle (α) of 60°, we can derive the relationship between the number of parallel channels (n) and the angles of the channels within the topological structure. As the number of channels increases, the differences between apex angles after formation of the topological structure also increase, indicating a reduction in the asymmetry of the V-shaped channels with the initial width of the SFOC (Fig. S11). Additionally, by fixing the number of channels (n) and the initial apex angle (α), introducing the folding angle (ϑ), we can establish the relationship between the apex angle (β) and the curling angle (ϑ). This reveals the varying values of different apex angles corresponding to different curling angles within the topological structure, thereby demonstrating the progressive asymmetrical transformation of the V-shaped channels from a flat sheet to a folding configuration in the topological SFOC. Consequently, this facilitates a more comprehensive analysis of the topological structure.

Supplementary Figures

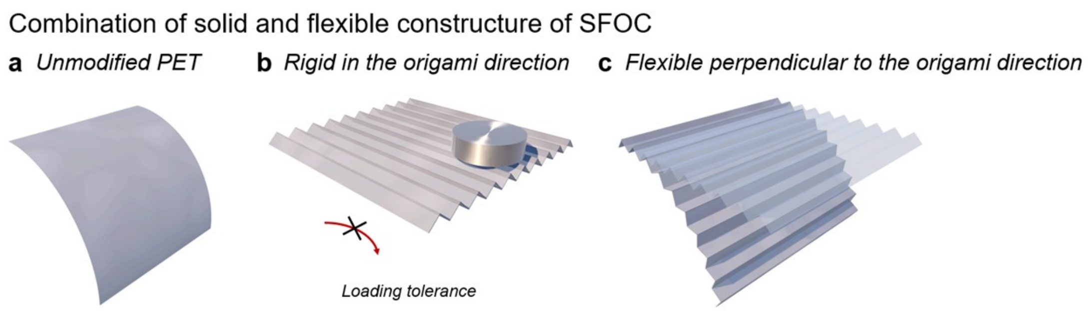

Fig. S1. The solid and flexible structure of SFOC. (a)Unmodified PET will bend under gravity. (b) The SFOC is rigid in the origami direction and flexible perpendicular to the origami direction (c).

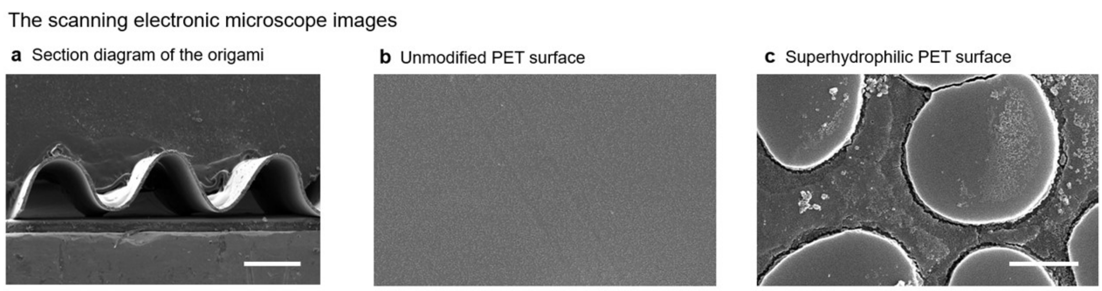

Fig. S2. The scanning electronic microscope (SEM) images of the section diagram of origami (a), the unmodified PET. Scale bar is 500 µm. (b) Superhydrophilic coating surface (c). Scale bar is 2 μm.

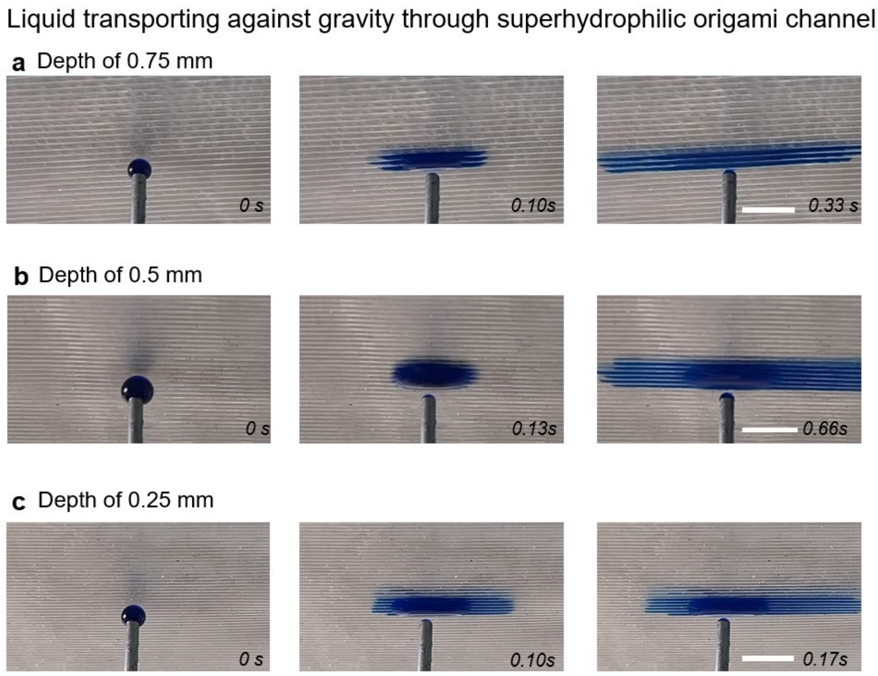

Fig. S3. The liquid self-pumping process of SFOC with varying depth against gravity. Scale bar is 5 mm.

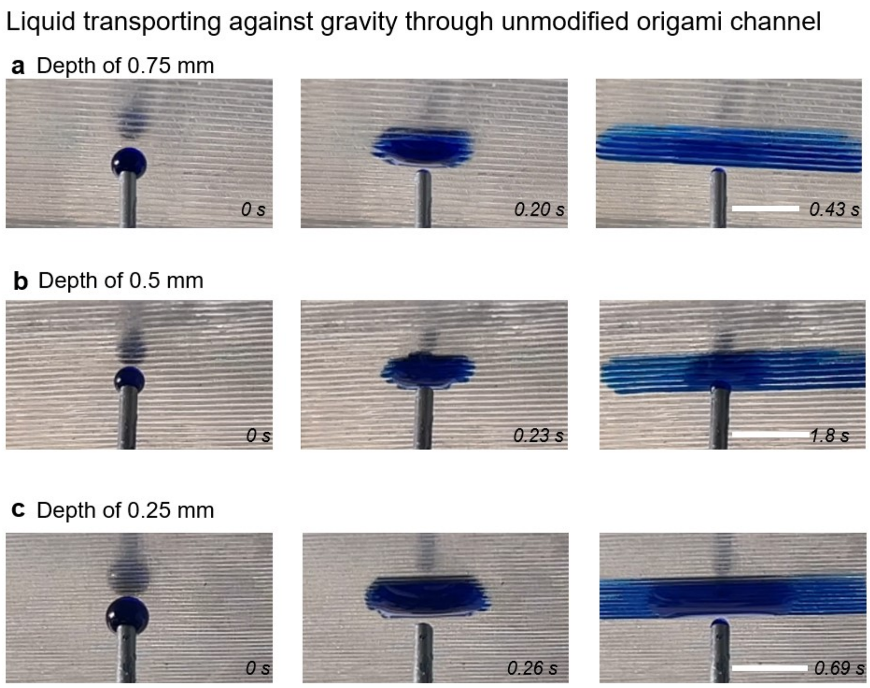

Fig. S4. The liquid self-pumping process of unmodified origami channel with varying depth against gravity. Scale bar is 5 mm.

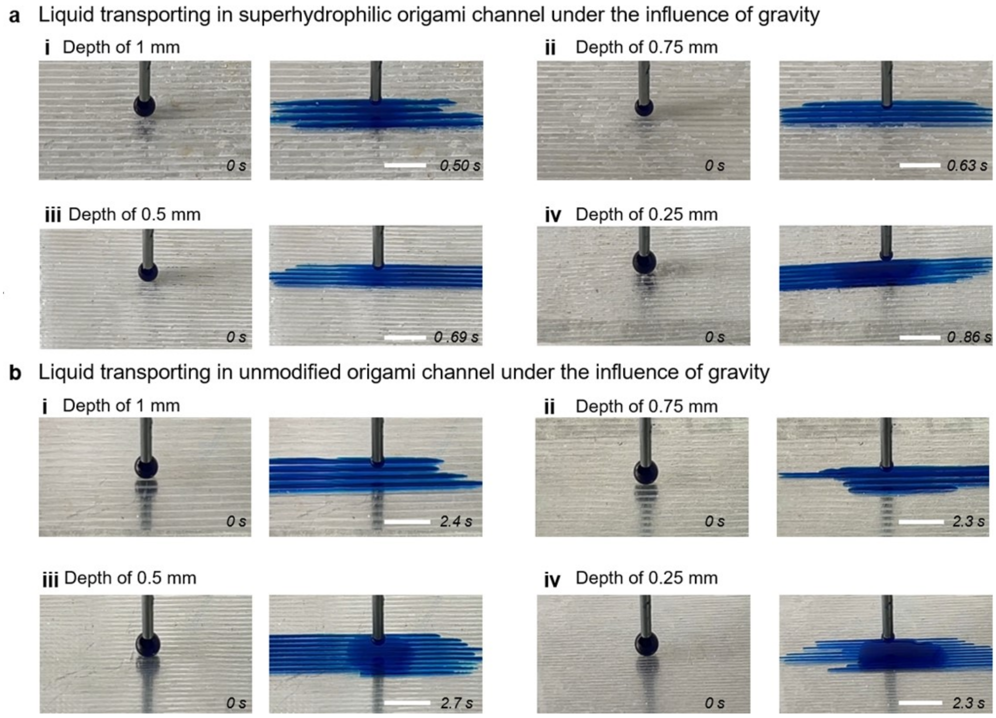

Fig. S5. The liquid transporting process in SFOC under gravity with different depth. Scale bar is 5 mm.

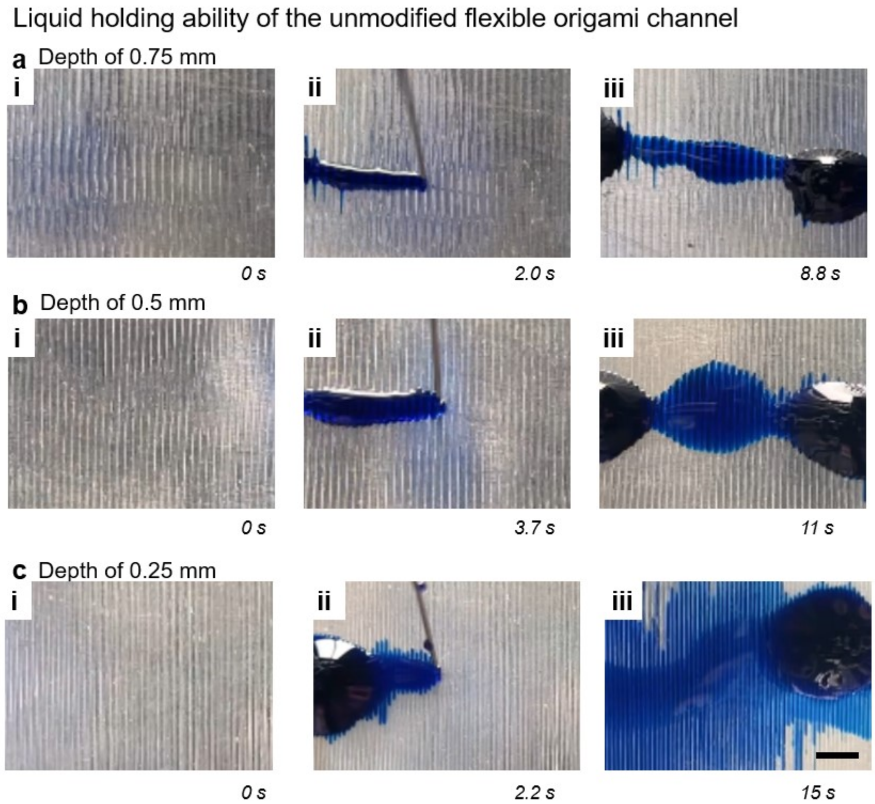

Fig. S6. The liquid holding ability of the unmodified origami channel against gravity. Scale bar is 5 mm.

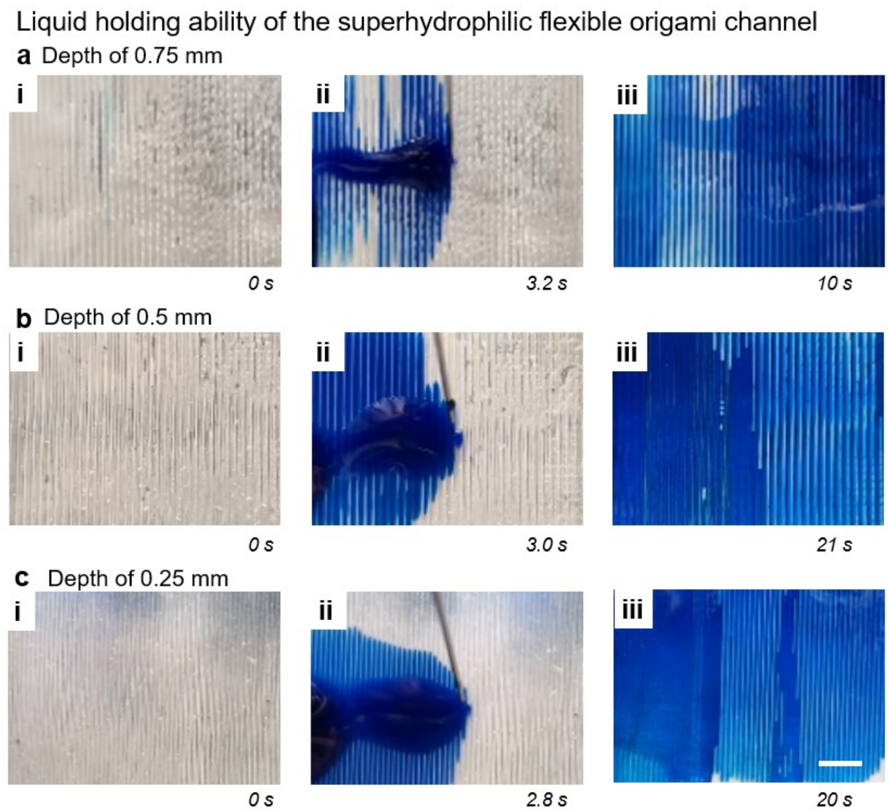

Fig. S7. The liquid holding ability of the SFOC against gravity with different depth of channel. Scale bar is 5 mm.

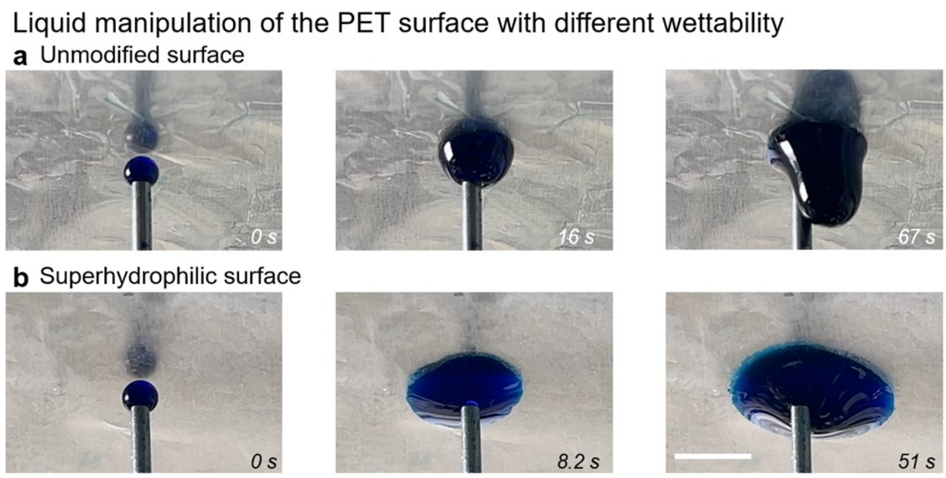

Fig. S8. The spreading process of PET surface with different wettability. Scale bar is 5 mm.

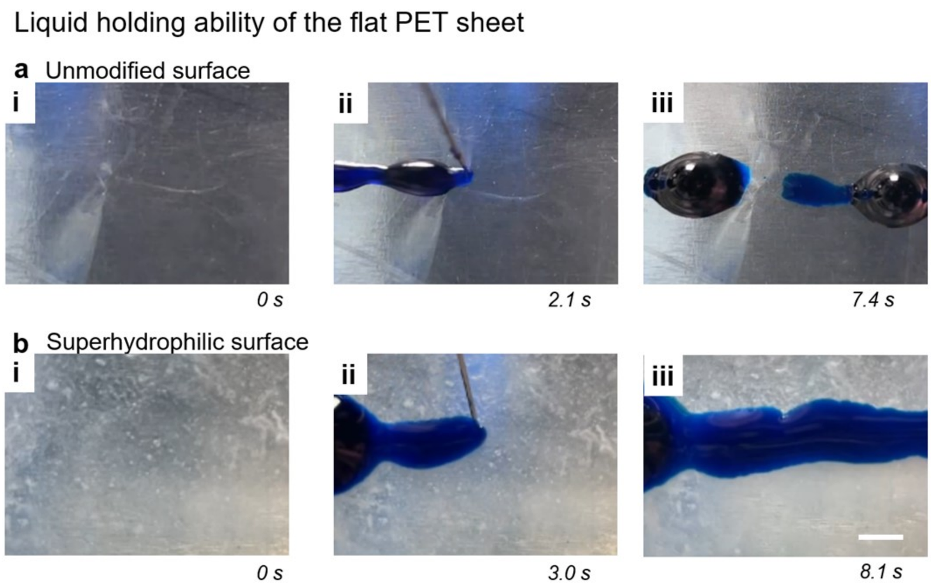

Fig. S9. The liquid holding ability of flat PET sheet with different wettability against gravity. Scale bar is 5 mm.

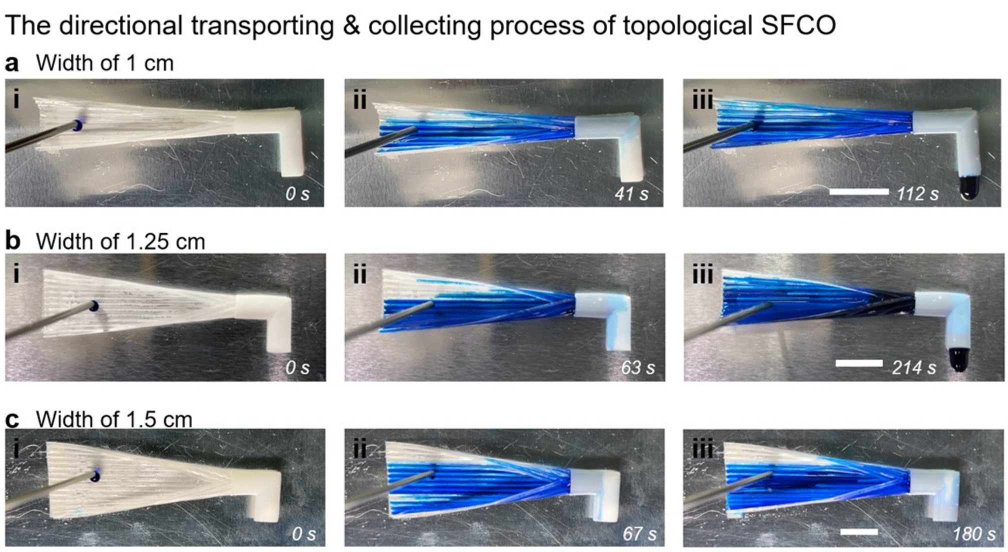

Fig. S10. The directional transporting ability and liquid collecting process of topological SFCO. Scale bar is 1 cm.

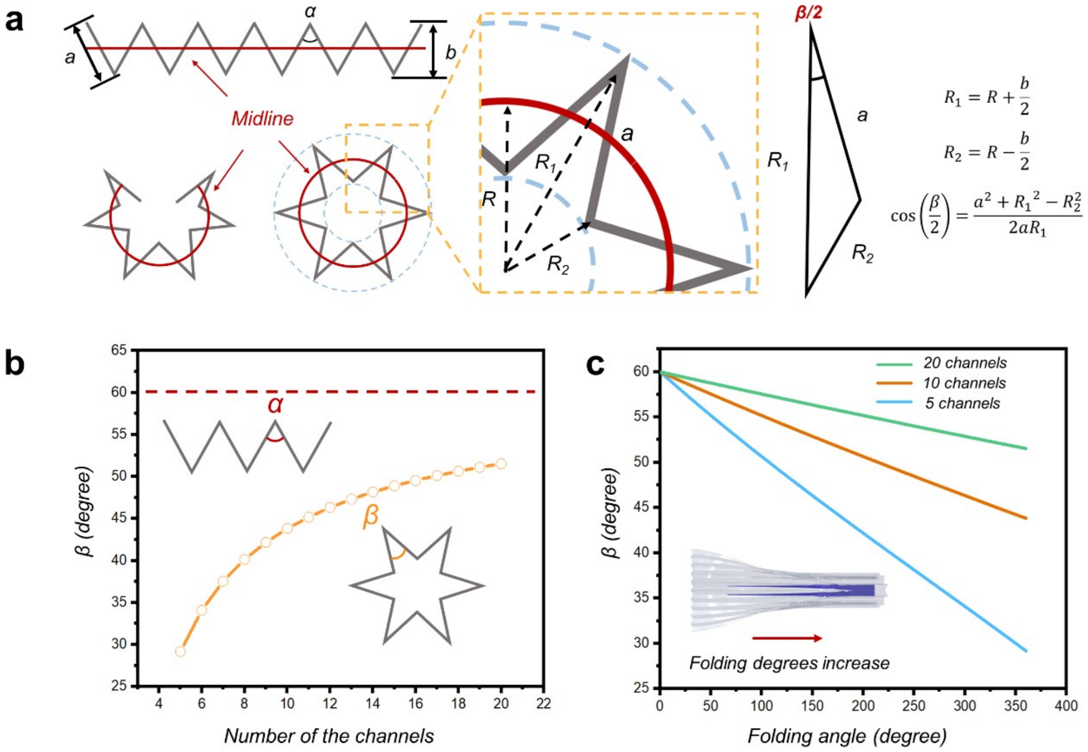

Fig. S11. The analysis of asymmetry channel after topological folding.

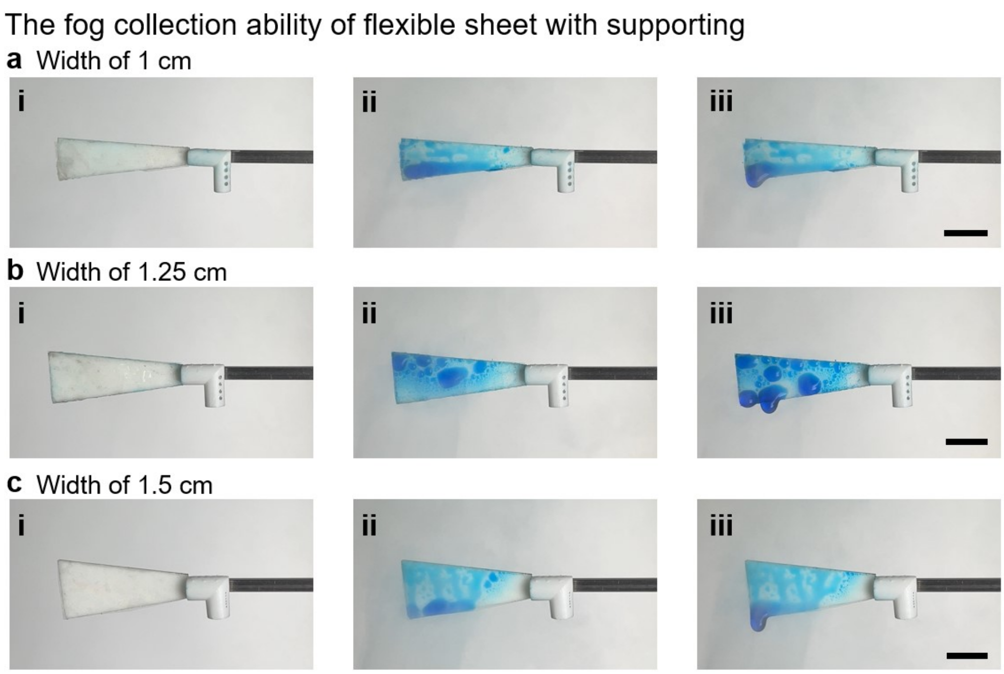

Fig. S12. The fog collecting ability of the flexible sheet with supporting. Scale bar is 1 cm.

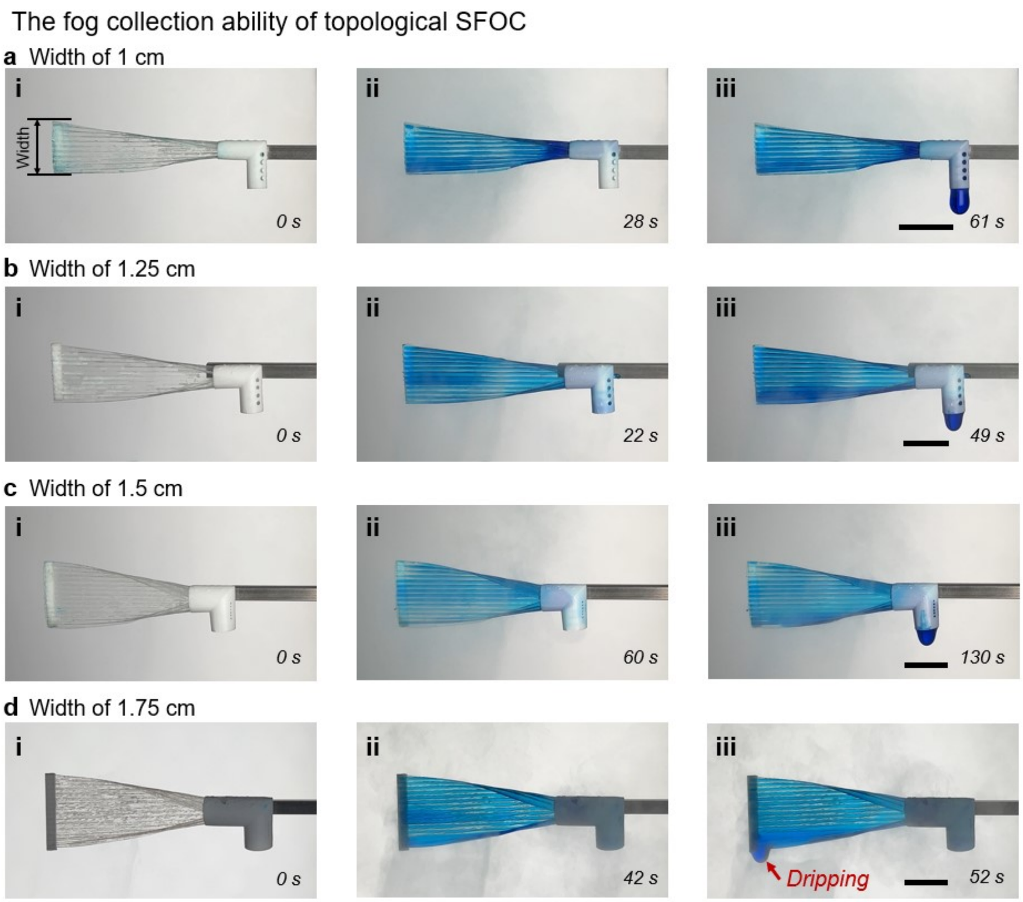

Fig. S13. The fog collecting ability of the topologic SFOC. Scale bar is 1 cm.

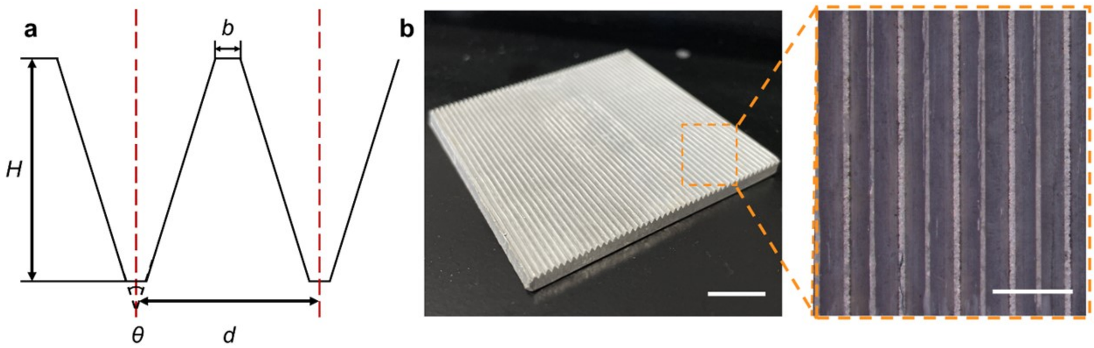

Fig. S14. The parameter and optical diagram of the aluminum mold, the scale bar of the optical diagram is 1 cm, while the scale bar of the optical microscope figure is 500 μm

Supplementary Movie:

Movie S1. Pumpless droplet transport in unmodified and superhydrophilic origami channels against gravity.

Movie S2. Liquid holding ability of unmodified and superhydrophilic origami channels against gravity.

Movie S3. Self-pumping and directional liquid transporting in the asymmetric SFOC.

Movie S4. Drop self-pumping and directional collecting process in topological SFOC.

Movie S5. Long distance pumpless liquid transport on the assembled SFOC.

Movie S6. The rigidity of SFOC system during the fog collection process.